Relationships Among Diurnal Variations of Polar Night Cloud, Precipitation, Surface Temperatures, and the Fair-Weather Return Current of the Global Electric Circuit (GEC)

Thomas Lavigne and Chuntao Liu

Department of Physical and Environmental Sciences, Texas A&M University-Corpus Christi

Submitted to Journal of Atmospheric Solar and Terrestrial Physics

February 2023

Keys words:

Global electric circuit, fair-weather electric field, stratified clouds, diurnal cycle, polar night temperature

Corresponding author address: Thomas Lavigne, Department of Physical and Environmental Sciences, Texas A&M University at Corpus Christi, 6300 Ocean Dr., Corpus Christi, 78412-5858

Email: tlavigne@islander.tamucc.edu

Abstract:

Over the past five years (June 2017-current), the vertical electric field (E_z) as well as numerous cloud, precipitation and radiation properties have been monitored at the Department of Energy-Atmospheric Radiation Measurement (DOE ARM) North Slope of Alaska (NSA) field site. Comparisons between the composite diurnal averaged fair-weather E_z, and composite ceilometer derived cloud base height during the polar night, reveal a significant correlation between the parameters ($r=0.62$), supporting previous studies that there is high correlation between local electric field and cloud properties. With the use of extensive instrumentation at the site, such as the Micro Pulse Lidar (MPL), Ka-band Zenith Radar (KAZR), ceilometer, SKYRAD, Precipitation Imaging Package (PIP), among others, this study provides a more comprehensive examination of the diurnal cycle of cloud and precipitation properties along with the localized fair-weather return current of the larger Global Electric Circuit (GEC) system. Comparisons between the composite diurnal averaged fair-weather E_z, and cloud thickness, maximum column backscatter, and precipitation particle counts all show similar diurnal variability during the polar night, indicating that during the largest magnitude fair weather E_z time periods, clouds bases tend to be higher, clouds are thicker, have a larger column backscatter, and display more precipitating particles. Furthermore, a slight diurnal variability in the polar night surface temperature was found to be highly correlated ($r=0.87$) to the longwave downwelling irradiance measured by SKYRAD, indicating that the variations in the physical properties of local clouds could modulate the diurnal polar night surface temperature variability on the order of 0.5ºC/day. These findings emphasize the importance and global nature of the GEC system, with the global aggregate of thunderstorms and electrified clouds potentially influencing polar night cloud properties as well as diurnal wintertime polar surface temperature variation.

Introduction:

1.1 The Global Electric Circuit (GEC) of the atmosphere.

The Global Electric Circuit (GEC) of the atmosphere is a naturally occurring phenomenon in which the Earth's atmosphere acts as a leaky capacitor between the Ionosphere and the Earth's surface [*Roble,* 1986; *Markson,* 2007; *Williams*, 2009; *Williams & Mareev*, 2014]. Primarily due to the constant presence of thunderstorms and electrified clouds around the globe, the leaky capacitor is continually recharged by the upward storm current produced above thunderstorms and electrified clouds [*Siingh et al*., 2007]. The balance between the fair-weather return current which drains the circuit, and the input from the upward storm current creates the stable Earth's electrical system known as the GEC.

Surface measurements of the vertical electric field (E_z) of the atmosphere have been conducted for more than one hundred years. [*Wilson,* 1909; *Wilson*, 1921; *Wilson*, 1924]. The most notable variability observed in the E_z is the evident diurnal cycle in UTC time observed at multiple locations around the globe in the absence of significant clouds, aerosols, and other local influences [*Harrison*, 2013; *Peterson et al*., 2017; *Nicoll et al*., 2019]. *Whipple* [1929], was the first to quantitively tie this diurnal variability of the E_z to the diurnal variability of global thunderstorm area in UTC time. Primarily driven by the differing numbers of thunderstorms and electrified clouds occurring globally in UTC time, the diurnal minimum in the E_z at 3:00 UTC, and the maximum at 19:00 UTC has been proven to be very consistent at many sites around the globe measuring fair-weather conditions, and is known as the Carnegie Curve [*Harrison*, 2013].

With the increased data availability of the satellite era, a clearer understanding of the amount and distribution global precipitation events and lightning activity became possible in comparison to the crude thunderstorm area gathered by ground stations in the early 20th century.

In the past several decades, more recent studies have now provided further evidence of the connection between the GEC and thunderstorm and electrified cloud activity on the diurnal [*Williams and Heckman*, 1993; *Williams*, 1994; *Adlerman and Williams*, 1996; *Mach et al*., 2011; *Blakeslee et al*., 2014], seasonal [*Burns et al.*, 2012; *Blakeslee et al*., 2014; *Lavigne et al*., 2017; *Lucas et al.,* 2017;], interannual [*Harrison, 2004*; *Burns & Frank-Kamenetsky, 2005; Markson*, 2007] and even possibly climate [*Williams*, 2005] timescales. The strongest magnitude GEC time periods have been observed to occur between June and October during the hours of 18-22 UTC, corresponding to the time-period of maximum global flash rates, as well as precipitation from thunderstorms and Electrified Shower Clouds (ESCs) [*Liu et al*., 2010; *Mach et al.,* 2011; *Lavigne et al*., 2017]. El Nino Southern Oscillation (ENSO) natural climate variability signals have also been observed in the GEC timeseries, indicating the potential ability of utilizing the variability of the GEC to observe changes in the climate system [*Harrison et al*., 2011; *Lavigne et al*., 2017; *Slyunyaev et al*., 2021].

1.2 Possible impacts of the GEC fair-weather return current.

As a clearer understanding of the battery that drives the GEC system becomes available, an interesting next question is how the system itself may influence the surrounding environment. A breakthrough study conducted by *Harrison and Ambaum* [2013], observed that in both the high latitude regions of the northern and southern hemisphere, a consistent diurnal variability of the cloud base height was present during the polar night time-period at each site. In both regions, persistent layered stratocumulus clouds are present for much of the polar night duration. The composite diurnal variability of this cloud base layer is consistent with the composite diurnal variability of the GEC, with the lowest cloud base heights occurring between 3-6 UTC, and the

maximum cloud base heights occurring between 19-20 UTC [*Harrison and Ambaum*, 2013]. The study also noted an inverse relationship between cloud base height and temperature anomalies with cooler air temperatures during periods with higher cloud base heights.

Nicoll and Harrison [2016], utilized specially instrumented radiosondes to measure the charge density and conductivity of the persistent layered stratocumulus clouds at Reading University in the United Kingdom. Results showed negative space-charge density at the cloud base, and positive space-charge density at the cloud top. The study showed that categorically all persistent layered clouds can be expected to contain charge at their cloud tops and bases due to the fair-weather return current of the GEC. However, it is also likely that a combination of the background electrical condition driven by the GEC, and cloud thermodynamics contribute to the magnitude of the charging of the cloud base and top [*Nicoll and Harrison*, 2016].

The presence of the fair-weather return current and the subsequent charging of the cloud top and bottom due to the conductivity difference between clear and cloudy air, is thought to potentially influence cloud microphysical processes such as droplet-droplet interactions, aerosol-droplet interactions as well as droplet activation [*Tinsley et al.,* 2000; *Khain et al.*, 2004; *Harrison & Ambaum* 2008; *Harrison*, 2015, *Nicoll & Harrison*, 2016]. The most likely effect is on the size and population of particles inside the charged layered clouds. This has implications for the radiation budget of the clouds, as well as the potential for increased precipitation activation [*Harrison et al*., 2015].

1.3 Multi-Year Electric Field Study-North Slope of Alaska (MYES-NSA) field campaign

In June 2017, the Multi-Year Electric Field Study-North Slope of Alaska (MYES-NSA) field campaign was established in Barrow, Alaska at the Department of Energy Atmospheric

Radiation Measurement (DOE ARM) site. The unique site provides the unprecedented ability to observe cloud, aerosol, and precipitation properties alongside surface E_z measurements [*Lavigne et al.,* 2021]. The field campaign location includes an upward pointing Ka-Band Radar, an upward pointing Micro Pulse Lidar (MPL), a ceilometer, two electric field mills, as well as numerous supplemental meteorological instrumentation [https://www.arm.gov/capabilities/observatories/nsa]. With the increased information regarding the cloud and aerosol properties of the layered clouds above the electric field meters (within 100m), it is conceivably possible to further understand the effects of the fair-weather return current magnitude on the properties of persistent layered clouds in the Arctic.

This manuscript aims to answer the following questions:

- Can the noteworthy relationship between the composite diurnal cycle of the fair-weather electric field and the composite polar night cloud base height, originally reported by *Harrison & Ambaum, [2013]*, be replicated in Barrow, AK?
- With the additional data available, are any other cloud or precipitation properties of long-lived stratified clouds observed to be modulated on a time scale similar to that of the GEC?
- How do the long-lived stratified clouds influence the diurnal change in surface temperature during the polar night in Barrow, AK?

2. Data and methodology:

The DOE ARM site located in the North Slope of Alaska (NSA) (71.2906° N, 156.7886° W) is a fully instrumented government facility which emphasizes on collecting data related to cloud and radiative processes at high latitudes [https://www.arm.gov/]. The NSA location

provides a unique opportunity to study the cloud and radiative properties in the Arctic, a location which is difficult to permanently maintain such a suit of instruments.

2.1 Ka-Zenith Radar (KAZR)

The site maintains a Ka-Band Zenith Radar (KAZR), which is a zenith pointing doppler radar that operates at the frequency of approximately 35 GHz. The KAZR has been in operation since 2011 and operates with a vertical resolution of 30 m from the near surface to 20 km, sampling every 3.5 seconds. The KAZR radar can measure the three Doppler moments; reflectivity, vertical velocity, and spectral width.

2.2 Micro Pulse Lidar (MPL)

The NSA facility also maintains a Micro Pulse Lidar (MPL), which operates at a wavelength of 532 nm and uses the same principle as a radar, measuring the backscattered energy back to the transmitter. The MPL has been in permanent operation at the NSA facility since 1998, and samples every 3 s with a vertical resolution of 30 m from the near surface to 20 km. The primary function of the MPL is to measure the aerosol backscattered radiation, total column backscatter ($km^{-1}*sr^{-1}$), as well as deriving the cloud base height.

2.3 Cloud Ceilometer

A ceilometer is also utilized to determine the cloud base height and has the ability to detect three cloud layers simultaneously. The ceilometer uses near infrared pulses and has a maximum vertical range of 7.7 km. With the ability of detecting the cloud top and bottom, a simple subtraction is utilized to determine the cloud thickness of the first layer. The backscatter

radiation can also be measured with the ceilometer. The ceilometer has been maintained on the NSA since 1997.

2.4 Laser Precipitation Monitor (LPM)

The Laser Precipitation monitor is an eye safe Distrometer that measures the drop size spectra and fall velocity of hydrometeors during precipitation events. The laser precipitation monitor measures the hydrometeor size distribution of precipitation events. The instrument can also detect the visibility, reflectivity at the surface, and the surface temperature, and has been in operation at the NSA site since April 2017.

2.5 Sky Radiometers on Stand For Downwelling Radiation (SKYRAD)

The Sky Radiometers on Stand For Downwelling Radiation (SKYRAD) is a collection of radiometers at the NSA site that measure longwave and shortwave irradiances. The SKYRAD radiometers collect data continuously and output every one-minute. Data recorded include longwave broadband downwelling irradiance, shortwave broadband diffuse downwelling irradiance, shortwave broadband direct normal irradiance, as well as cloud fraction. The suit of sky rad instruments has been operating at the NSA site since 1999.

2.6 Campbell Scientific Electric Field Meter (CS110)

Two Campbell Scientific CS110s have been deployed at the NSA site since 2017 in conjunction with the Multi Year Electric field Study at Northern Slope Alaska (MYES-NSA) field campaign [Lavigne et al. 2021]. The CS110s sample at a rate of 1 Hz, with a maximum measurement range of +/-20,000 V/m. A slight vertical profile is present between the two

CS110's, with one instrument mounted at 2 m and the other at 5 m above the surface. Both CS110s have been calibrated to the ground level with the use of a 3rd ground flush upward facing CS110 [*Chmielewski,* 2013]. This also calibrates out the bending of the vertical field lines caused by the surrounding metal towers and mounting materials (see *Lavigne et al.,* [2021] for more details). Both CS110s are located less than 100 m from all the other coordinating instrumentation mentioned above. Fair-weather time periods are determined using the method outlined in *Lavigne et al.* [2021], utilizing 5-minute time periods with an averaged standard deviation of less than 15 V/m, and mean E_Z values between -250 V/m to -50 V/m. This criterion was determined with the help of the MPL and KAZR, and largely excludes time periods with high aerosol concentrations or significant clouds. Through extensive analysis, this fair-weather definition has been shown to remove time periods with extensive cloud and aerosol activity.

Throughout this manuscript, the fair-weather E_z is represented as positive values. As the accepted standard, the direction of an electric field is the path a positive test charge would take if it were exposed to the force of the field, leading to a negative electric field under fair-weather conditions. However, for ease of visualization, as well as maintaining consistency with previous literature, the fair-weather electric field is shown as the absolute value of the measured electric field. For this reason, all fair-weather electric fields throughout the manuscript are shown as positive values.

2.7 Polar Night Time Period, Diurnal Averaging and Binning

The polar night occurs in Barrow, Alaska each year for 66-days between the dates of November 18th and January 22nd. With the absence of incoming solar radiation, the polar night time period acts as a unique laboratory-like setting to observe smaller magnitude diurnal

variability not caused by the diurnal solar cycle. Only data from 2017-2022 occurring in the polar night time period in Barrow, Alaska is used in this analysis.

For diurnal comparison, 9 selected variables MPL and ceiliometer derived cloud base height MPL cloud thickness, MPL total column backscatter, LPM precipitation intensity and number of precipitation particles, LPM visibility, surface air temperature, SKYRAD longwave downwelling irradiance, CS110 vertical electric field) are binned in hourly averages. Simple Pearson correlation coefficients are calculated between all variables to determine statistical correlation.

2.8 Comparison between the composite diurnal fair-weather electric field and composite cloud and radiation properties in Barrow, Alaska.

All analysis throughout this manuscript compares the composite diurnal fair-weather electric field, to the composite averaged cloud, radiation, and temperature parameters. It is important to note, that this is not a simultaneous comparison between the fair-weather E_z and the various localized parameters. Following *Lavigne et al.,* [2021], rigorous steps were taken to remove time periods with significant cloud or aerosol contribution when defining a fair-weather time-period. This allows for a single station to compare the relationship among the diurnal variations of polar night cloud, precipitation, surface temperatures, and the diurnal fair-weather E_z. All variables are binned to 1-hour means for the diurnal analysis. Simple Pearson correlation coefficients (r-values) are then calculated between all variables.

3. Results

3.1 Cloud base height, cloud top height, and cloud thickness verses the fair-weather vertical electric field at the NSA site.

In a past study, the Cloud Base Height (CBH) was compared to the magnitude of the fair-weather vertical electric field at high latitude sites in both the Northern (Sodankylä, Finland) and Southern (Hailey, Antarctica) Hemispheres [*Harrison & Ambaum*, 2013]. Results from both locations show a similar relationship between the composites of the two variables thousands of kilometers away when measured during their polar night time period. With the addition of another polar site measuring the electric field in Barrow, Alaska, a similar comparison between the CBH and fair-weather E_z is worthwhile to determine the global nature of this phenomena.

Figure 1a shows the diurnal variability of the measured composite fair-weather electric field in Barrow, Alaska (red), the CBH (solid), the cloud top height (CTH) (dashed), and the cloud thickness (dotted) measured by the MPL located at the NSA site during the polar night time period. Cloud thickness is calculated as the simple subtraction of the cloud top minus cloud base of the first layered cloud in the column measured the MPL. All timeseries are binned to 1-hourly averages and are computed as a percent deviation from the mean value during the sampled period. A similar diurnal pattern is observed in Figure 1a between all four variables, comparable to that observed in Harrison & Ambaum, [2013], with the peak in both the E_z and the CBH occurring between 16 and 19 UTC. A clear statistical positive correlation is present between the CBH and fair-weather E_z, with a Pearson correlation of 0.74 and a p-value of $4.05e^{-5}$. The magnitude is also comparable between the diurnal composites of the three cloud properties and the fair-weather E_z during the polar night. However, the cloud properties do observe slightly larger magnitudes of diurnal variation with a minimum occurring at approximately 12-14 UTC

and maxima at 17-19 UTC. Interestingly, a peak is observed in the CBH between 5-9 UTC, which is not displayed in the E_z diurnal cycle. The mismatch during this period deserves further exploration in the future.

Figure 1a also shows that when CBH, CTH, cloud thickness and the fair-weather Ez variables are directly compared, a potential diurnal propagation is observed in the diurnal maxima, with the polar night fair weather E_z peaking first at 16 UTC, the CBH peaking 1-hour later at 17 UTC, followed by the cloud thickness peaking at 17-18 UTC. This propagation could imply that the properties of the long-lived stratified clouds in the polar night may indicate that the influence of the magnitude of the E_z may take several hours to fully influence the clouds. The CBHs and CTHs tend to continue to grow in the column for approximately an hour after the E_z peaks, and the clouds continue to become thicker for approximately 2-hours after the E_z peaks. This finding warrants further investigation in the future.

Figure 1b shows the yearly-averaged composite diurnal variability of the measured fair-weather electric field in Barrow, Alaska (red), the CBH (solid), the cloud top height (CTH) (dashed), and the cloud thickness (dotted) measured by the ceilometer located at the NSA site. A clear regime change is observed in comparison to the polar night time period (1a). The yearly-averaged fair-weather electric field is completely out of phase with the composite CBH, CTH, and thickness, with the peak in GEC occurring at 20 UTC, and the peak in CBH occurring at 5-6 UTC. This peak in CBH corresponds to the minima time-period of the GEC. This result indicates that the CBH, CTH and cloud thickness observe a similar diurnal phase and amplitude only during the polar night in Barrow, AK without the influence of incoming solar shortwave radiation.

With the unprecedented ability to observe the properties of the aerosols and clouds above the measured ground-based electric field, comes the opportunity to explore the relationship between the fair weather E_z and other properties of the long-lived stratified clouds that occur in the polar night in Barrow, Alaska. Figure 2a shows a two-dimensional histogram of the cloud fraction observed during the polar night in Barrow Alaska by the KAZR radar. A threshold of -30 dBZ is applied to determine cloud verses no-cloud conditions. The threshold value -30 dBZ is used to be consistent with the CloudSat cloud detection sensitivity [*Stephens et al*., 2002]. The cloud fraction is calculated by dividing the observed number of clouds in each KAZR time and height bin, by the total number of sampled bins for each corresponding time and height. A similar diurnal pattern as previously mentioned is observed in the cloud fraction measured by the KAZR. Clouds heights tend to trend towards lower in the column from 0 UTC to approximately 5 UTC. The clouds then start to trend higher in the column exhibiting a peak around 15 UTC, corresponding to the peak in thunderstorm and electrified clouds from the African convective chimney [*Williams & Satori*, 2004; *Mach et al*., 2011] . The clouds then continue to trend higher in the column, peaking between 4-5 km between 19-22 UTC, agreeing with the peak strength period of the fair-weather E_z. Figure 2a also displays that clouds tend to occur with a larger magnitude variation of heights (possibly indicating thickness) during the early UTC hours, and peaking later between 20-22 UTC, corresponding to a similar result shown in Figure 1.

Figure 2b shows a two-dimensional histogram of cloud base counts observed by the laser ceilometer located at the NSA site. Cloud base counts were calculated by taking the cumulative number of CBH heights observed by the ceilometer observed at each time and height throughout the polar night. Results are comparable to Figure 2a and show the majority of the long-lived stratified clouds occur with a cloud base at approximately 2,000 m between 2-10 UTC. Cloud

base counts increase to 2,500 to 3,000 m later in the UTC time, peaking during 19-22 UTC. This is consistent with both the diurnal fraction of cloud counts measured by the KAZR, as well as the time of maxima fair-weather E_z. The dashed black line represents the hourly-averaged mean CBH for the entire sampled period. The corroboration of two cloud monitoring instruments, the KAZR and laser ceilometer, provide stronger evidence that the CBHs and cloud thickness during the polar night are indeed in similar phase and amplitude as the simultaneous magnitude of the fair-weather E_z which is known to be primary driven by global thunderstorm and electrified cloud activity.

Figure 3 shows the two-dimensional diurnal histogram of MPL backscatter ($km^{-1}*sr^{-1}$) derived aerosol event counts during the polar night in Barrow, Alaska during the years of 2017-2022. A threshold of 100 $km^{-1}*sr^{-1}$ was applied to determine an aerosol/no aerosol event period. Below 200 m, the aerosol fraction is very high, with a nearly uniform diurnal cycle observing significant aerosol 40% or more of the day. Above 250 m, the aerosol fraction decreases significantly to less than 0.1. Again, no significant diurnal cycle is indicated in the aerosol fraction aloft, indicating that the majority of aerosols occur in the lower 250 m and are uniform throughout the day. This indicates that the concentration of aerosol aloft at the near-surface is not in phase with the GEC, and is primarily driven by other factors, such as surface wind and anthropogenic activity.

3.2 Cloud precipitation and optical properties verses vertical fair-weather electric field at the NSA site.

The supplementary suit of instrumentation at the NSA site in Barrow, Alaska, allows for further investigation into the optical and precipitation properties of polar night clouds in Barrow,

and how they potentially relate to the fair-weather E_z. Figure 4a shows the diurnal cycle of the composite fair-weather E_z (solid) and the composite diurnal cycle of number of falling precipitation particles (dashed) measured at the surface with the laser precipitation distrometer. Both variables are analogous in both phase and amplitude. During periods of maxima fair weather E_z values, there tends to be more falling precipitation particles. It is important to point out that these two variables are not measured simultaneously and are composites of the entire sampled period. For example, time periods of falling precipitation are very likely removed from the fair-weather E_z definition, therefore the time periods of falling precipitation are compared to the climatology of fair-weather in Barrow, Alaska in the lack of precipitation, clouds, aerosol, etc.

Figure 4b displays a similar diurnal pattern of composite total column backscatter. The sum backscatter variable ($km^{-1}*sr^{-1}$) is measured as the total accumulation of backscatter in the column observed by the ceilometer. In agreement with the number of precipitation particles, the sum backscatter displays remarkable phase agreement to the diurnal cycle of E_z. However, the sum backscatter does observe a slightly smaller diurnal magnitude.

Figure 4c shows the diurnal variation of the composite precipitation intensity (dashed) compared to the fair-weather E_z (solid). A much less consistent relationship is observed between the two variables in comparison to number of precipitation particles and sum backscatter to the fair-weather E_z. However, the minima and maxima in precipitation intensity do align within 1-hour with the diurnal E_z. The precipitation intensity diurnal amplitude is twice as large as the fair-weather Ez. A further investigation is needed to verify if the two parameters are indeed physically linked.

3.3 Relationship between the longwave downwelling, fair weather E_z and cloud base height

Figure 5 explores the relationship between the longwave downwelling irradiance emitted from the polar night clouds, and the composite fair-weather E_z as well as CBH. Figure 5a displays the scatter plot of the longwave downwelling from the polar night clouds and ambient air, and the fair-weather E_z. A clear statistically significant negative correlation is present with a Pearson correlation of -0.70. There is an approximate 1 W/m drop in longwave downwelling for every increase in 5 V/m in the fair-weather E_z.

Figure 5b shows the relationship between the CBH and longwave downwelling. Again, the figure displays a robust negative relationship between the two variables. A statistically significant relationship is present with a Pearson correlation of -0.63. As the CBHs form lower in the column, there tends to be less longwave downwelling irradiance measured by the *SKYRAD.* These relationships shown in Figure 5, indicate that the amount of longwave downwelling irradiance measured at the surface is statistically related to the intensity of the fair-weather E_z, due to its effect on the long-lived stratified CBH formation in the column. Since there is no incoming solar shortwave radiation during the polar night, this variability in longwave downwelling irradiance from the clouds is more pronounced, and potentially influential on the radiation budget of the region.

Figure 6a shows the diurnal variation of the measured surface temperature (solid) and the longwave downwelling irradiance (dashed) during the polar night time-period measured during the years of 2017-2022. A striking inter-timestep variability is present between the two variables, with a Pearson correlation of 0.87. This indicates that during the polar night, the largest influence on the diurnal variation of surface temperature in Barrow is the longwave downwelling irradiance emitted from the persistent clouds as well as ambient air. Without the influence of any

incoming solar shortwave radiation, there is still a 0.5° C diurnal variability in surface air temperature. As noted in *Harrison & Ambaum*, 2013 as well as supported by Figure 1, the formation of the CBH is directly related to the intensity of fair-weather E_z. This supports the finding that the diurnal variability of surface temperature in Barrow during the polar night could be driven by the intensity of the GEC. This connects the summation of all global thunderstorm and electrified clouds to the temperature variability in the polar night Arctic.

Figure 6b shows that during the non-polar night time period in Barrow, AK, the surface temperature (solid) is no longer in phase with the longwave downwelling irradiance measured at the surface (dashed). This diurnal phase is also inconsistent with the well-known diurnal GEC such as in the case of the figure 6a. This mismatch indicates that the surface temperature during the non-polar night time periods is not driven by GEC, and rather the obvious incoming radiation from the sun. This drastic diurnal phase change in the surface temperature and longwave downwelling irradiance indicates a clear regime change in the drivers of diurnal temperature variability in the polar-night Arctic. With the diurnal variability of CBH, CTH, cloud thickness, as well as other precipitation properties at the NSA site supporting the findings of *Harrison & Ambaum*, [2013], the GEC theory influencing persistent stratified clouds in the Arctic polar-night deserves more attention as a potential leading candidate for this observed diurnal variability of cloud and precipitation properties during the Arctic polar-night.

4. Summary and Discussion:

In the laboratory-like setting during the 66-days of polar night in Barrow, Alaska, the influence of the sun's emitted shortwave radiation on the diurnal cycle of clouds, precipitation, aerosols, and surface temperature is considered minimal-to-none [*Lüpkes et al*., 2008]. This

offers the opportunity to observe smaller magnitude effects that may influence the diurnal variability of these parameters globally, which may go undetected and unrepresented in the understanding of the climate system. Observations during the 5-years of collected E_z, cloud, precipitation, and aerosol data at the NSA site during the polar night, show that the CBH, CTH, cloud thickness, number of precipitating particles, total column backscatter, and surface temperature are modulated on timescales consistent with the diurnal variation exhibited in the GEC system.

Figure 7 summarizes the correlation matrix between the composites of all explored polar night cloud and precipitation variables; cloud thickness, (c. thickness) longwave downwelling (DLWI), fair-weather E_z, CBH, sum column backscatter (sum backscatter), number of precipitation particles (particles (#)), precipitation intensity (precip intensity), temperature, and visibility. Warm colors indicate positive linear correlations between the variables, and cool colors indicate negative linear correlations of the hourly averaged diurnal timeseries. The largest positive correlations (r-values >0.75) occur between the surface temperature and longwave downwelling irradiance, as well as the precipitation intensity and the surface reflectivity. Other statistically significant positive correlations (r-value > 0.5 & r-value < 0.75), occur between the sum of the column backscatter and the fair-weather E_z, CBH and the fair-weather E_z, and sum of the column backscatter and number of precipitation particles. Other polar night cloud and precipitation properties show smaller, but still statistically significant (r-value >0.25 & r-value < 0.5) are present between the fair-weather E_z and the cloud thickness, number of precipitating particles, and the visibility.

Figure 7 shows the most negatively correlated parameters (r-values < -0.5) between the fair-weather E_z and the surface temperature, fair-weather E_z and longwave downwelling, and the

longwave downwelling and CBH. All correlations that are between plus or minus 0.25 are shown as white, as they are less statistically significant.

Figure 8 summarizes these results in a schematic diagram. Figure 8a and Figure 8b display the composite mean 5 UTC polar night and 17 UTC scenarios respectively in Barrow, Alaska. Results from this study, building off the works of *Harrison & Ambaum* [2013] among several others, shows that during time periods in the polar night with larger magnitude electric fair-weather electric fields (GEC return current), the persistent layered clouds in Barrow Alaska tend to have higher CBHs, CTHs, tend to be thicker, precipitate with more numerous particles, have less longwave downwelling irradiance, leading to slightly cooler surface temperatures (approximately 0.5^{o} C colder). The opposite effect on these properties occurs for time periods of relatively small magnitude fair-weather E_z. Figure 8 shows that during 17 UTC, the mean surface E_z is 16.6 V/m greater than the mean E_z at 5 UTC. This also corresponds to mean CBHs that form approximately 230 m higher in the column as well as grow 240 m thicker during the average 17 UTC condition when compared to the average 5 UTC time-period. Precipitation events tend to precipitate approximately 5 particles/second more during 17 UTC in comparison to 5 UTC events. The persistent layered clouds that form closer to the ground during 5 UTC emit 1.62 W/m^2 more longwave downwelling irradiance, than 17 UTC conditions, leading to a slightly warmer surface temperature (0.4^{o}C) than during average 17 UTC temperatures.

These results indicate that in the lack of incoming solar shortwave radiance during the polar night, these cloud parameters modulate on the GEC diurnal timescale. This leads to the speculation that the totality of thunderstorms and electrified clouds transpiring around the globe, directly influence the diurnal cloud and precipitation properties as well as surface temperature in the high latitude regions of the globe during the polar night. The electrical effect on cloud

formation and precipitation modulation remains a large uncertainty in climate models. This GEC effect needs to be included, especially in the polar regions, to model the climate system more accurately.

Major finding from this study include:

- A statistically significant relationship is found between the CBH formation in Barrow, Alaska (>71°N), and the composite magnitude of the fair-weather E_z (r-value = 0.61) during the polar night time periods. This result corroborates the findings in Finland and Antarctica, displaying a similar relationship on the GEC diurnal timescale.
- During the polar night, the composite fair-weather E_z is also found to be statistically correlated to the CTH, cloud thickness, sum of the column backscatter, the number of precipitation particles at the surface, the longwave downwelling irradiance, and the surface temperature. During periods of larger magnitude fair-weather E_z (more global thunderstorms and electrified clouds), the clouds tend to be taller, thicker, have a larger total column backscattering, and have more numerous precipitating particles at the surface.
- A significant linear relationship is present between the composite fair-weather E_z and the longwave downwelling irradiance from the persistent clouds in Barrow (r-value = -0.70). An even more correlated relationship between the diurnal longwave downwelling irradiance and the surface temperature (r-value = 0.87) is found in the region. This implies that as the CBHs occur higher in the vertical column during larger magnitude fair-weather E_z time periods, there tends to be less longwave downwelling from the clouds, which leads to colder surface temperatures. This

provides evidence that the diurnal surface temperature variability observed during the polar night could be indirectly related to the magnitude of the GEC current driven by global thunderstorms and electrified clouds.

Thirty-to-forty percent of the globe is covered by persistent stratocumulus clouds with liquid particles, a slightly different from to those in ice phase explored in this study [*Nicoll & Harrison*, 2016]. Although the GEC effect on these clouds in the tropics and subtropics, which never experience the polar night may be much smaller than the effect of the diurnal solar incoming radiance, it may not be negligible on the cloud physics and precipitation properties of these clouds. Future work is needed to better understand the how the presence of the GEC return current, occurring continually all over the globe, influences the properties of global clouds. This could indeed provide an important piece of the climate system, that is not very well understood presently.

5. Acknowledgement:

This study was supported by NSF-2219639. Thanks to the support of DOE ARM program allowing the setup of the instruments at NSA site. Thanks to Walter, Jimmy, Josh, Ross among many others for the support and maintenance of instruments at the NSA site over the years. All NSA CS110 data are available at DOE ARM Site at:
https://adc.arm.gov/discovery/#/results/iopShortName::nsa2017oyesnsa
As well as at Texas A&M Corpus Christi website: http://atmos.tamucc.edu/oyesnsa/data/

6. References

Adlerman, E. J., & Williams, E. R. (1996). Seasonal variation of the global electrical circuit. *Journal of Geophysical Research: Atmospheres*, **101(D23)**, 29679-29688.

Blakeslee, R. J., Mach, D. M., Bateman, M. G., & Bailey, J. C. (2014). Seasonal variations in the lightning diurnal cycle and implications for the global electric circuit. *Atmospheric research*, ***135***, 228-243.

Burns, G. B., Frank-Kamenetsky, A. V., Troshichev, O. A., Bering, E. A., & Reddell, B. D. (2005). Interannual consistency of bi-monthly differences in diurnal variations of the ground-level, vertical electric field. *Journal of Geophysical Research: Atmospheres*, *110*(D10).

Burns, G. B., Tinsley, B. A., Frank-Kamenetsky, A. V., Troshichev, O. A., French, W. J. R., & Klekociuk, A. R. (2012). Monthly diurnal global atmospheric circuit estimates derived from Vostok electric field measurements adjusted for local meteorological and solar wind influences. *Journal of the atmospheric sciences*, *69*(6), 2061-2082.

Chmielewski, V. C. (2013). *Variations of the vertical electric field and wind speed on days with airborne dust in Lubbock, Texas* (Doctoral dissertation).

Harrison, R. G. (2004). Long-range correlations in measurements of the global atmospheric electric circuit. *Journal of atmospheric and solar-terrestrial physics*, *66*(13-14), 1127-1133.

Harrison, R. G. (2013). The carnegie curve. *Surveys in Geophysics*, *34*(2), 209-232.

Harrison, R. G., & Ambaum, M. H. (2008). Enhancement of cloud formation by droplet charging. *Proceedings of the Royal Society A: Mathematical, Physical and Engineering Sciences*, *464*(2098), 2561-2573.

Harrison, R. G., Joshi, M., & Pascoe, K. (2011). Inferring convective responses to El Niño with atmospheric electricity measurements at Shetland. *Environmental Research Letters*, *6*(4), 044028.

Harrison, R. G., & Ambaum, M. H. (2013). Electrical signature in polar night cloud base variations. *Environmental Research Letters*, *8*(1), 015027.

Harrison, R. G., Nicoll, K. A., & Ambaum, M. H. P. (2015). On the microphysical effects of observed cloud edge charging. *Quarterly Journal of the Royal Meteorological Society*, *141*(692), 2690-2699.

Khain A, Arkhipov V, Pinsky M, Feldman Y, Ryabov Y. 2004. Rain enhancement and fog elimination by seeding with charged droplets. Part I: Theory and numerical simulations. J. Appl. Meteorol.43: 1513 – 1529.

Lavigne, T., Liu, C., Deierling, W., & Mach, D. (2017). Relationship between the global electric circuit and electrified cloud parameters at diurnal, seasonal, and interannual timescales. *Journal of Geophysical Research: Atmospheres*, *122*(16), 8525-8542.

Lavigne, T., Liu, C., Hill, J., & Bruning, E. (2021). Observations from the one year electric field Study-North Slope of Alaska (OYES-NSA) field campaign, and their implications for observing the distribution of global electrified cloud activity. *Journal of Atmospheric and Solar-Terrestrial Physics*, *214*, 105528.

Liu, C., Williams, E. R., Zipser, E. J., & Burns, G. (2010). Diurnal variations of global thunderstorms and electrified shower clouds and their contribution to the global electrical circuit. *Journal of the atmospheric sciences*, *67*(2), 309-323.

Lucas, G. M., Thayer, J. P., & Deierling, W. (2017). Statistical analysis of spatial and temporal variations in atmospheric electric fields from a regional array of field mills. *Journal of Geophysical Research: Atmospheres*, *122*(2), 1158-1174.

Lüpkes, C., Vihma, T., Birnbaum, G., & Wacker, U. (2008). Influence of leads in sea ice on the temperature of the atmospheric boundary layer during polar night. *Geophysical Research Letters*, *35*(3).

Mach, D. M., Blakeslee, R. J., & Bateman, M. G. (2011). Global electric circuit implications of combined aircraft storm electric current measurements and satellite-based diurnal lightning statistics. *Journal of Geophysical Research: Atmospheres*, *116*(D5).

Markson, R. (2007). The global circuit intensity: Its measurement and variation over the last 50 years. *Bulletin of the American Meteorological Society*, *88*(2), 223-242.

Nicoll, K. A., & Harrison, R. G. (2016). Stratiform cloud electrification: comparison of theory with multiple in-cloud measurements. *Quarterly Journal of the Royal Meteorological Society*, *142*(700), 2679-2691.

Nicoll, K. A., Harrison, R. G., Barta, V., Bor, J., Brugge, R., Chillingarian, A., ... & Yaniv, R. (2019). A global atmospheric electricity monitoring network for climate and geophysical research. *Journal of atmospheric and solar-terrestrial physics*, *184*, 18-29.

Peterson, M., Deierling, W., Liu, C., Mach, D., & Kalb, C. (2017). A TRMM/GPM retrieval of the total mean generator current for the global electric circuit. *Journal of Geophysical Research: Atmospheres*, *122*(18), 10-025.

Roble, R. G. (1986). The global atmospheric-electrical circuit. *The Earth's electrical environment*, 206-231.

Siingh, D., Gopalakrishnan, V., Singh, R. P., Kamra, A. K., Singh, S., Pant, V., ... & Singh, A. K. (2007). The atmospheric global electric circuit: an overview. *Atmospheric Research*, *84*(2), 91-110.

Slyunyaev, N. N., Ilin, N. V., Mareev, E. A., & Price, C. G. (2021). The global electric circuit land–ocean response to the El Niño—Southern Oscillation. *Atmospheric Research*, *260*, 105626.

Stephens, G. L., Vane, D. G., Boain, R. J., Mace, G. G., Sassen, K., Wang, Z., ... & Mitrescu, C. (2002). The CloudSat mission and the A-Train: A new dimension of space-based observations of clouds and precipitation. *Bulletin of the American Meteorological Society*, *83*(12), 1771-1790.

Tinsley, B. A., Rohrbaugh, R. P., Hei, M., & Beard, K. V. (2000). Effects of image charges on the scavenging of aerosol particles by cloud droplets and on droplet charging and possible ice nucleation processes. *Journal of the atmospheric sciences*, *57*(13), 2118-2134.

Whipple, F. J. W., 1929: On the association of the diurnal variation of electric potential gradient in fine weather with the distribution of thunderstorms over the globe. Quart. J. Roy. Meteor. Soc., 55, 1–17.

Williams, E. R. (1994). Global circuit response to seasonal variations in global surface air temperature. Monthly Weather Review, 122(8), 1917–1929. https://doi.org/10.1175/1520-0493(1994)1222.0.CO;2

Williams, E. R. (2005). Lightning and climate: A review. *Atmospheric research*, *76*(1-4), 272-287.

Williams, E. R. (2009). The global electrical circuit: A review. *Atmospheric Research*, *91*(2-4), 140-152.
Williams, E. R., & Heckman, S. J. (1993). The local diurnal variation of cloud electrification and the global diurnal variation of negative charge on the Earth. *Journal of Geophysical Research: Atmospheres*, *98*(D3), 5221-5234.
Williams, E. R., & Sátori, G. (2004). Lightning, thermodynamic and hydrological comparison of the two tropical continental chimneys. *Journal of Atmospheric and Solar-Terrestrial Physics*, *66*(13-14), 1213-1231.
Williams, E., & Mareev, E. (2014). Recent progress on the global electrical circuit. *Atmospheric Research*, *135*, 208-227.
Wilson, C. T. R. (1909). LVI. On thunderstorm electricity. *The London, Edinburgh, and Dublin Philosophical Magazine and Journal of Science*, *17*(100), 634-641.
Wilson, C. T. R. (1921). III. Investigations on lighting discharges and on the electric field of thunderstorms. *Philosophical Transactions of the Royal Society of London. Series A, Containing Papers of a Mathematical or Physical Character*, *221*(582-593), 73-115.
Wilson, C. T. R. (1924). The electric field of a thundercloud and some of its effects. *Proceedings of the Physical Society of London (1874-1925)*, *37*(1), 32D.

Figures:

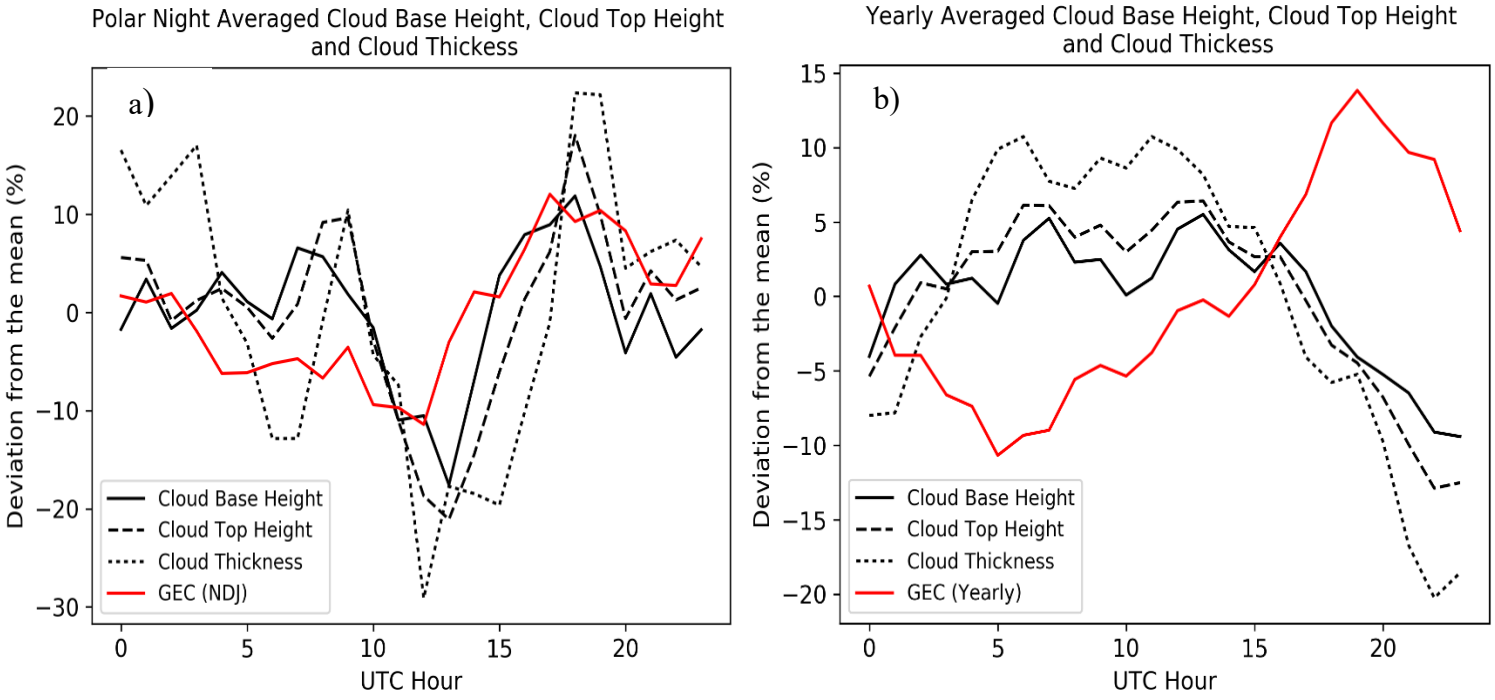

Figure 1: Diurnal variations of the a) polar-night and b) yearly averaged fair weather electric field (red), cloud-base height (solid), cloud top height (dashed), and cloud thickness (dotted) measured with the Micro-Pulse Lidar (MPL) in Barrow AK during the years of 2017-2022.

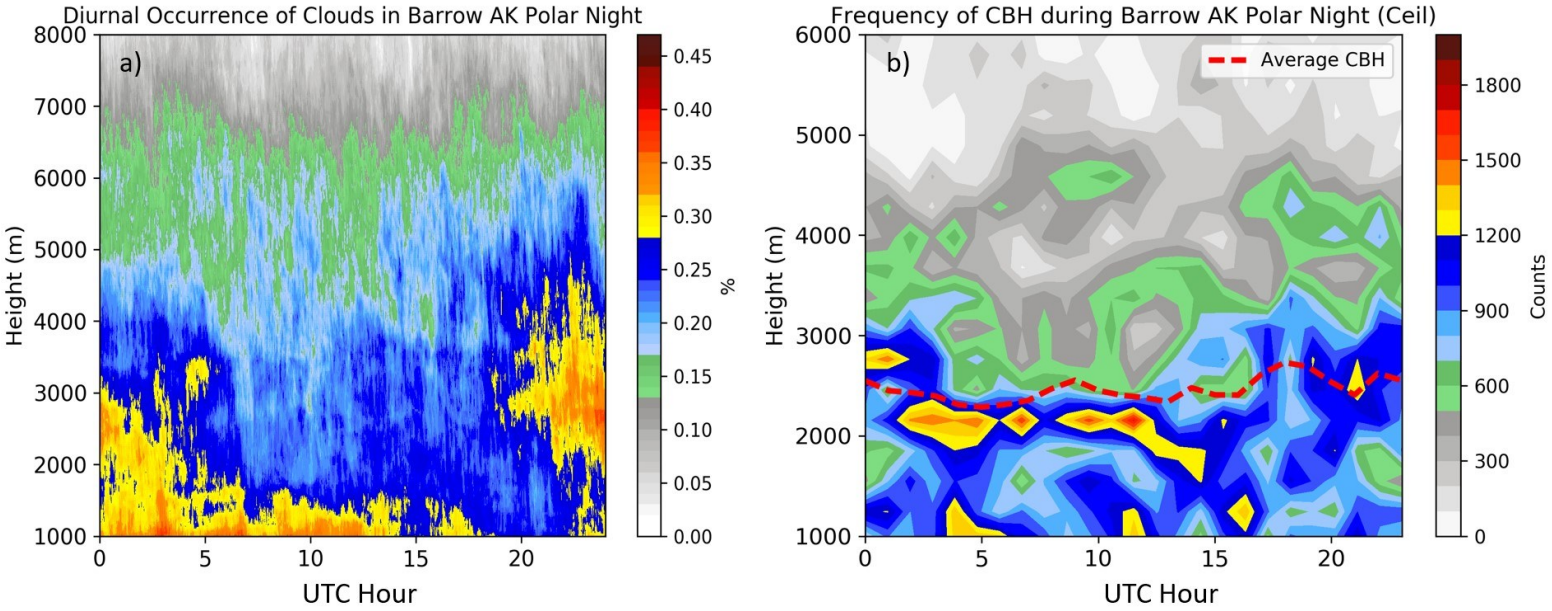

Figure 2: a) Two-Dimensional histogram of polar night cloud occurrence (%) in Barrow, Alaska measured by the Ka-Band Zenith Radar (KAZR). A threshold of -30 dBZ was used to determine the presence/absence of a cloud. b) Two-Dimensional histogram of polar night cloud counts in Barrow, Alaska measured by the ceilometer. The dashed black line is the mean cloud base height during the same time-period binned to 1-hour averages.

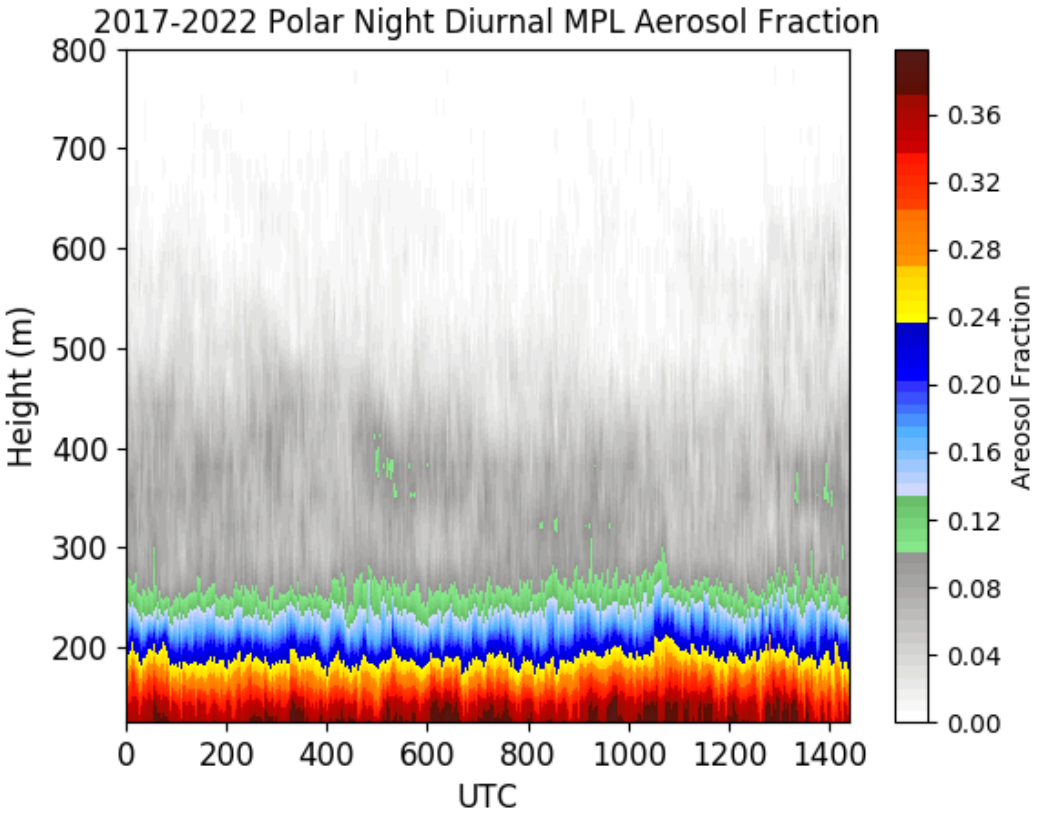

Figure 3: Two-Dimensional histogram of polar night aerosol occurrence (%) in Barrow, Alaska measured by the Micro Pulse Lidar (MPL). A threshold of 100 km-^{1}*sr-^{1} was used to determine the presence/absence of an aerosol event.

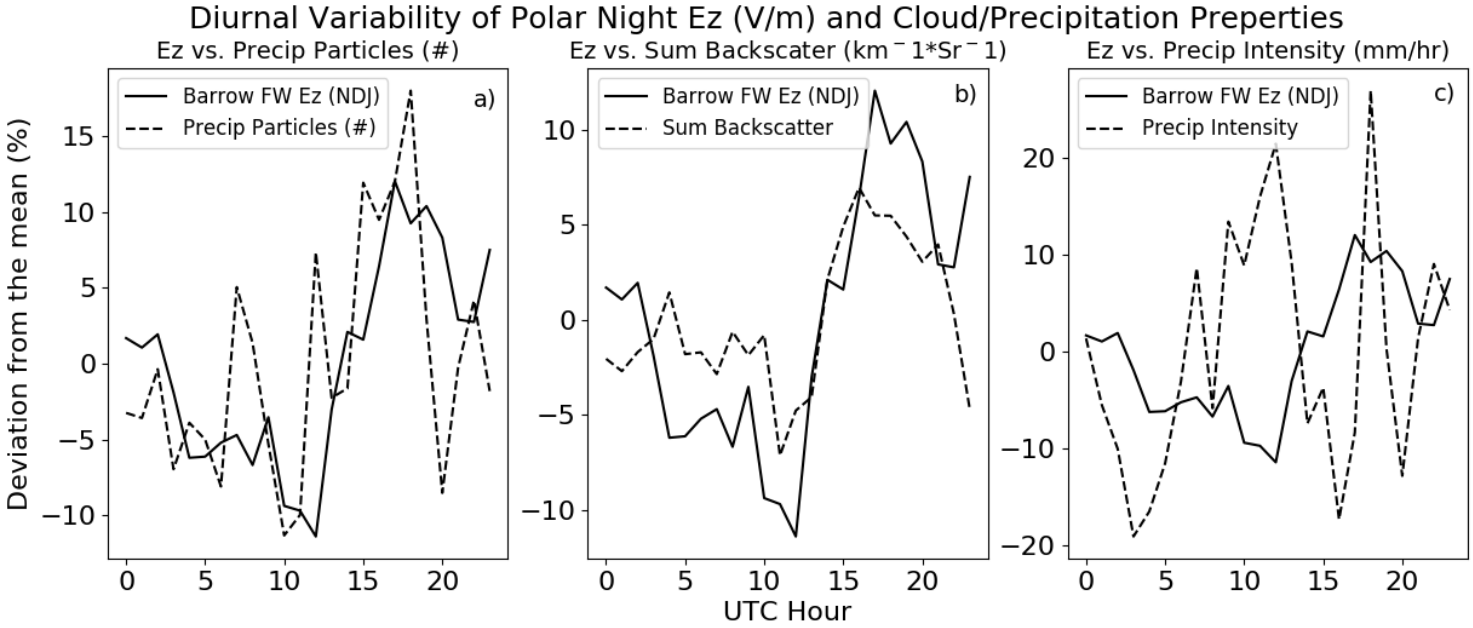

Figure 4: a) Diurnal variation of the polar-night averaged fair weather electric field (solid), and polar night cloud precipitation particle counts (dashed) measured with the impact distrometer. b) Diurnal variability of the polar-night averaged fair weather electric field (solid), and polar night cloud sum of vertical column backscatter (dashed) measured with the micro-pulse Lidar. c) Diurnal variability of the polar-night averaged fair weather electric field (solid), and polar night cloud precipitation intensity (dashed) measured with the impact distrometer. All values are normalized as a percent deviation from the mean value during polar night in Barrow AK for the years of 2017-2021.

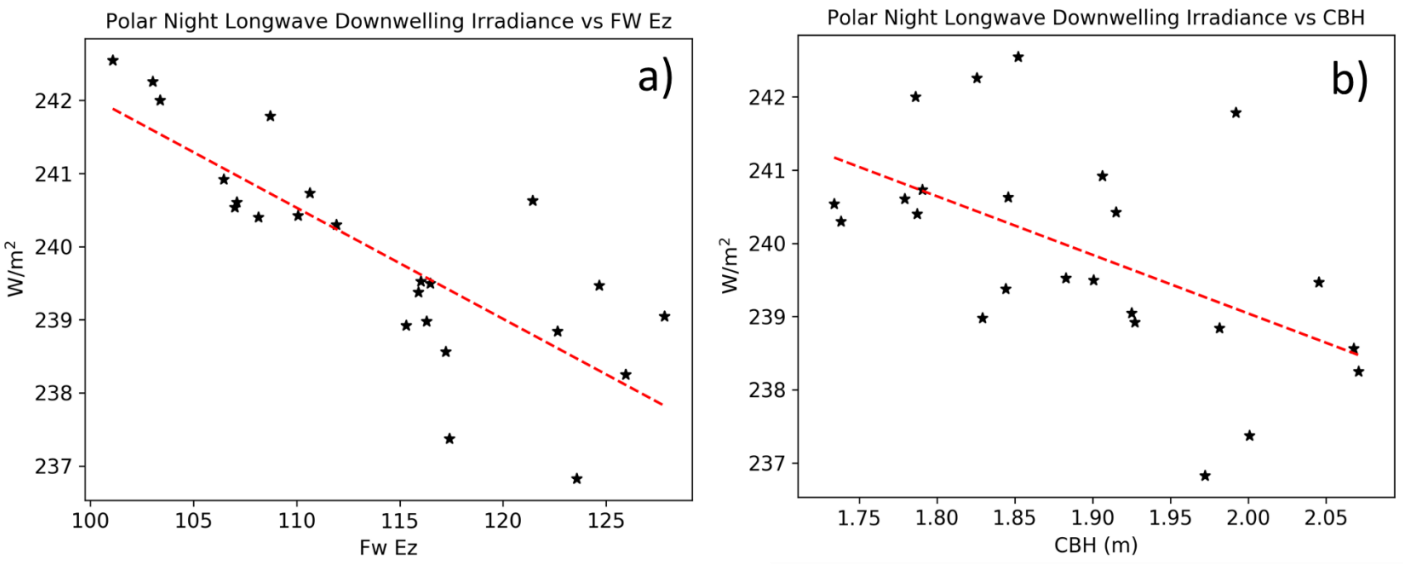

Figure 5: a) Scatter plot of hourly average of the polar night fair weather electric field (V/m), verses downwelling longwave irradiance (W/m^2). b) Scatter plot of hourly average of the Cloud Base Height (km), verses downwelling longwave irradiance (W/m^2). Measurements were made in Barrow AK during the polar night in 2017-2022.

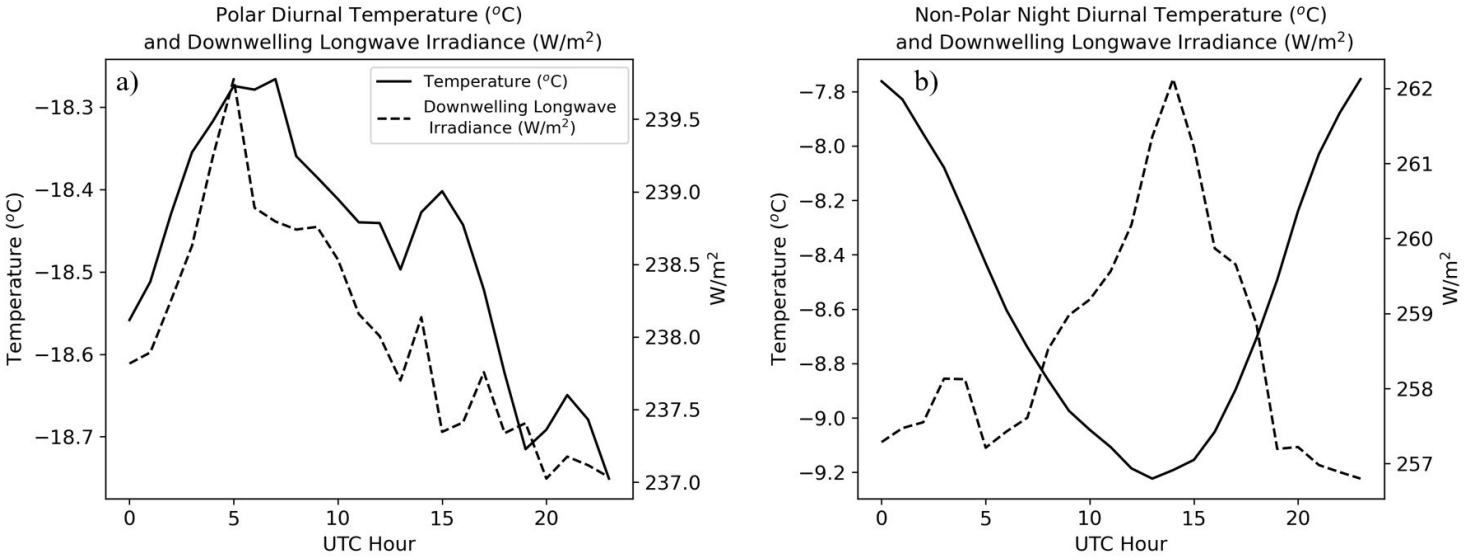

Figure 6: Diurnal variation of the polar night (a) and non-polar night (b) surface air temperature (solid) and downwelling longwave irradiance (dashed) measured by the SKYRAD during the years of 2017-2022.

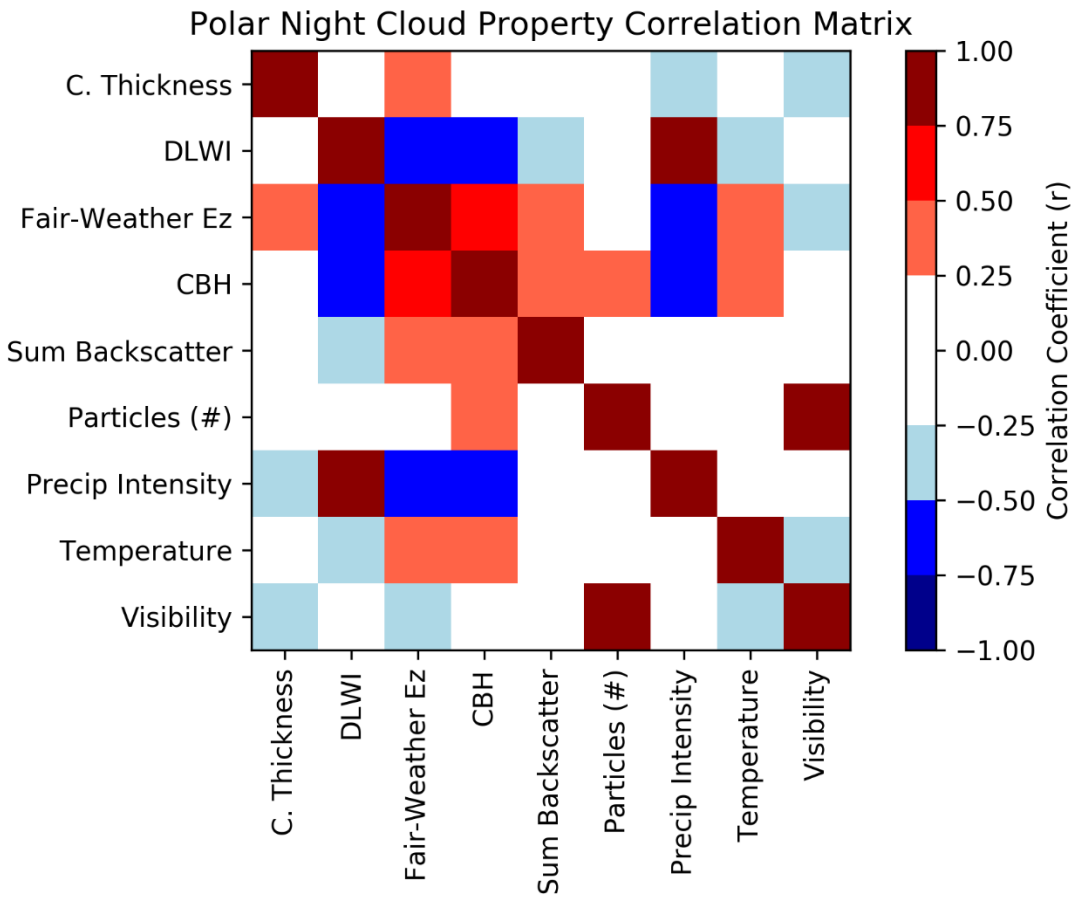

Figure 7: Correlation matrix of the diurnal variability of 9-explored polar night properties: cloud thickness (c. thickness), downwelling longwave irradiance (DLWI), fair-weather E_z, cloud base height (CBH), sum of vertical backscatter (sum backscatter), number of precipitation particles (particles (#), precipitation intensity, temperature, and visibility. All correlations that are between plus or minus 0.25 are shown as white, as they are less significant.

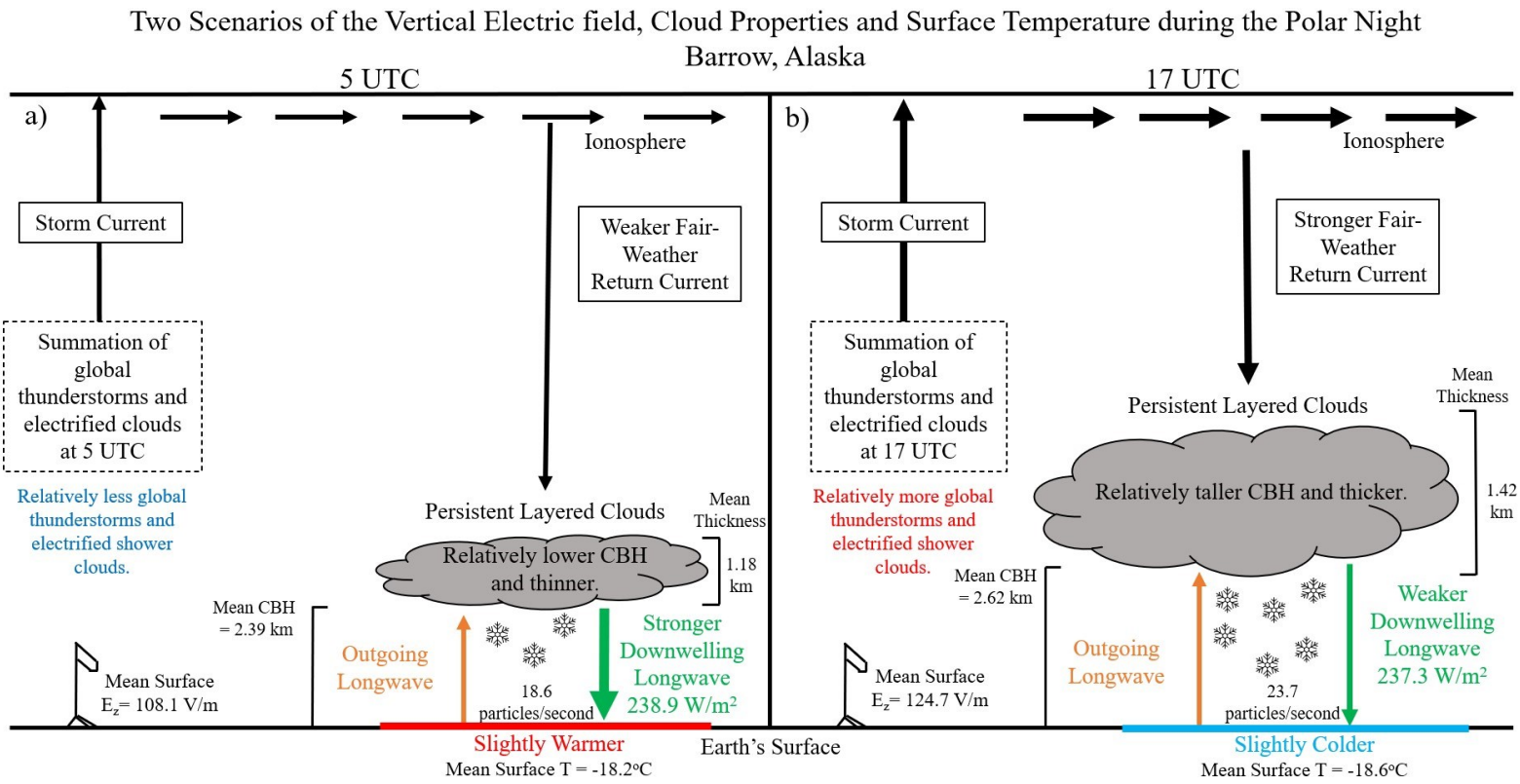

Figure 8: Summary schematic of the influence of the GEC on diurnal properties of persistent layered clouds and diurnal variation of surface temperature during the polar night.